Electronic structure and polar catastrophe at the surface of Li_{x}CoO_{2} studied by angle-resolved photoemission spectroscopy

Y. Okamoto, R. Matsumoto, T. Yagihara, C. Iwai, K. Miyoshi, J. Takeuchi, K. Horiba, M. Kobayashi, K. Ono, H. Kumigashira, N. L. Saini, and T. Mizokawa

Phys. Rev. B **96**, 125147 — Published 25 September 2017

DOI: 10.1103/PhysRevB.96.125147

Electronic structure and polar catastrophe at surface of Li_xCoO_2 studied by angle-resolved photoemission spectroscopy

Y. Okamoto,[1] R. Matsumoto,[1] T. Yagihara,[1] C. Iwai,[2] K. Miyoshi,[2] J. Takeuchi,[2] K. Horiba,[3] M. Kobayashi,[3] K. Ono,[3] H. Kumigashira,[3] N. L. Saini,[4] and T. Mizokawa[1]

[1]*Department of Applied Physics, Waseda University, Shinjuku, Tokyo 169-8555, Japan*

[2]*Department of Material Science, Shimane University, Matsue 690-8504, Japan*

[3]*Institute of Materials Structure Science, High Energy Accelerator Research Organization (KEK), Tsukuba, Ibaraki 305-0801, Japan*

[4]*Department of Physics, University of Roma "La Sapienza" Piazzale Aldo Moro 2, 00185 Roma, Italy*

(Dated: August 2, 2017)

Abstract

We report an angle-resolved photoemission spectroscopy (ARPES) study of Li_xCoO_2 single crystals which have a hole-doped CoO_2 triangular lattice. Similar to Na_xCoO_2, the Co 3*d* a_{1g} band crosses the Fermi level with strongly renormalized band dispersion while the Co 3*d* e'_g bands are fully occupied in Li_xCoO_2 (x=0.46 and 0.71). At x=0.46, the Fermi surface area is consistent with the bulk hole concentration indicating that the ARPES result represents the bulk electronic structure. On the other hand, at x=0.71, the Fermi surface area is larger than the expectation which can be associated to the inhomogeneous distribution of Li reported in the previous scanning tunneling microscopy study by Iwaya *et al.* [Phys. Rev. Lett. **111**, 126104 (2013)]. However, the Co 3*d* peak is systematically shifted towards the Fermi level with hole doping excluding phase separation between hole rich and hole poor regions in the bulk. Therefore, the deviation of the Fermi surface area at x=0.71 can be attributed to hole redistribution at the surface avoiding polar catastrophe. The bulk Fermi surface of Co 3*d* a_{1g} is very robust around x=0.5 even in the topmost CoO_2 layer due to the absence of the polar catastrophe.

PACS numbers: 71.28.+d, 79.60.-i, 73.20.At

I. INTRODUCTION

Li_xCoO_2 has been widely used as an electrode material in commercial Li ion batteries [1–4]. Li_xCoO_2 has the layered α-$NaFeO_2$ structure (space group $R\bar{3}m$) in which the CoO_2 layers and the Li layers are alternatingly stacked along the c axis. [5] In the CoO_2 layer, the CoO_6 octahedra share their edges and form the two-dimensional Co triangular lattice as shown in Fig. 1(a). While the Li ions occupy the octahedral sites between the CoO_2 layers in Li_xCoO_2, the well studied Na_xCoO_2 has a similar structure with different staking sequence in which the Na ions are in the prismatic sites between the CoO_2 layers. The electronic structure of Na_xCoO_2 has been intensively investigated in order to understand the origins of the good thermoelectric properties, [6] the superconductivity in the hydrated compound $Na_{0.35}CoO_2{\cdot}1.3H_2O$ below $T_c \sim 5$K, [7] and the interesting low temperature phase diagram as a function of x. [8–10] X-ray absorption spectroscopy (XAS) studies on Na_xCoO_2 and related systems [11–13] have established that both Co^{3+} and Co^{4+} have the low-spin t_{2g}^6 and t_{2g}^5 configurations, respectively, with the trigonal ligand field splitting of triply degenerate t_{2g} into the a_{1g} and doubly degenerate e_g' states [Fig. 1(b)]. The ARPES studies [14–22] revealed that the doped holes are accommodated by the a_{1g} band and that the circular hole pocket is formed around the Γ point. The a_{1g} band is strongly renormalized with large effective mass, and Geck *et al.* have assigned the strong band renormalization to the inter-orbital Coulomb interactions and magnetic correlations. [18]

Compared to Na_xCoO_2, number of electronic structural studies on Li_xCoO_2 is rather small due to the difficulty of growing single crystals. $LiCoO_2$ is a nonmagnetic insulator with Co^{3+} low-spin state (t_{2g}^6). [23–26] By removing the Li ions using an electrochemical reaction, Li_xCoO_2 exhibits an insulator-to-metal transition at around x=0.95 by hole doping in the t_{2g} band. [27, 28] Single crystals of Li_xCoO_2 were successfully synthesized by Miyoshi *et al.* [29, 30] and their electronic structure has been studied by photoemission spectroscopy, [31] x-ray absorption spectroscopy, [32] and hard x-ray absorption and emission spectroscopy. [33] In particular, the x-ray absorption study has revealed that the a_{1g} band with strong mixture of O $2p$ accommodates the doped holes and that the O $2p$ hole plays an important role for the Li-ion motion in Li_xCoO_2. [32]

It has recently found that surface of Li_xCoO_2 exhibits micro-scale inhomogeneous distribution of insulating and metallic regions by means of scanning tunneling microscopy (STM).

[34] In addition, the STM study revealed that a small fraction of the cleaved surface is covered by Li and the subsurface CoO_2 layer is insulating. On the other hand, most of the imaged surface is the metallic CoO_2 layer with hole concentration larger than the bulk hole concentration. [34] If the Li^+ ions are homogeneously distributed in the bulk and the crystal is cleaved at the Li layer, half of the Li ions remain at the cleaved surface in a homogenous or inhomogeneous manner as illustrated in Fig. 1(c) or 1(d). In this context, an interesting question is whether the surface CoO_2 layer of Li_xCoO_2 has a Fermi surface similar to that reported in Na_xCoO_2 or not. It is highly interesting to study the bulk and surface electronic structure of Li_xCoO_2 with strong inhomogeniety and to compare it to that of Na_xCoO_2. In the present work, in order to reveal the electronic structure of Li_xCoO_2 in the momentum space, we have performed ARPES of single crystals. At x=0.46, the area of the a_{1g} Fermi surface is consistent with the bulk hole concentration and the effect of inhomogeniety is limited. On the other hand, at x=0.71, the Fermi surface area is larger than the expectation indicating the inhomogeneous distribution of Li and the surface charge redistribution for avoiding polar catastrophe.

II. EXPERIMENT

Single crystals of Li_xCoO_2 with x=0.71, 0.46, and 0.25 were prepared as reported by Miyoshi *et al.* [29, 30] The ARPES measurements were performed at beamline 28A of Photon Factory, KEK using a SCIENTA SES-2002 electron analyzer with circularly polarized light. The total energy resolution was set to 25-30 meV for the excitation energies from $h\nu = 60$ eV to $h\nu = 70$ eV. The angular resolution was set to $\sim 0.2^\circ$ that gives the momentum resolution of 0.014 $Å^{-1}$ for $h\nu = 70$ eV. The base pressure of the spectrometer was in the 10^{-9} Pa range. The single crystals were cleaved *in situ* in order to obtain clean surfaces at 20 K. The ARPES spectra were acquired at 20 K within 12 hours after the cleaving. The Fermi level was determined using the Fermi edge of clean gold reference samples.

III. RESULTS AND DISCUSSION

Figure 2 exhibits a Fermi surface map for x=0.46 taken at $h\nu = 70$ eV. The Fermi surface map is obtained by plotting ARPES intensity integrated within ± 5 meV from the Fermi

level (E_F) as a function of in-plane wave numbers k_x and k_y. The out-of-plane wave number k_z is approximately given by 4.37 Å^{-1} ($\sim 6.5\times\pi/c$) for $h\nu = 70$ eV. A Fermi surface centered at the Γ point is clearly observed. The band maps indicate that the Fermi surface is created by the hole-like band with very small band dispersion near E_F. Such a hole-like Fermi surface was reported in Na_xCoO_2 which has extensively been studied by APRES [14–19]. In the ARPES studies on Na_xCoO_2, the hole-like band at E_F was assigned to the Co 3d a_{1g} orbital with strong mixture of O 2p. Considering the similarity between Na_xCoO_2 and Li_xCoO_2, it is reasonable to assign the hole-like Fermi surface in Li_xCoO_2 to the Co 3d a_{1g} orbital. The Fermi surface area is estimated by extrapolating the observed Fermi surface considering the six-fold symmetry of Li_xCoO_2 crystal. The extrapolated Fermi surface is almost circular and can be fitted to a circle with radius of 0.71 ± 0.03 $\mathring{A}^{-1}$. Since the observed Fermi surface is hexagonally distorted from an ideal circle, the upper limit of the radius is set to cover the Fermi surface while the circle with the radius in the lower limit is included in the Fermi surface. The Fermi surface area is estimated to be $\sim$ 1.58 ± 0.15 $\mathring{A}^{-2}$. Assuming that the Fermi surface does not depend on the out-of-plane wave number k_z, the estimated area is consistent with the area expected from the Li content (1.55 $\mathring{A}^{-2}$) that is obtained by multiplying the first Brillouin zone area by (1-x)/2. Indeed, Fermi surface areas observed at photon energies of 60 eV and 150 eV are similar to that obtained at 70 eV supporting the assumption. This agreement with the theoretical estimation indicates that the hole concentration of the surface CoO_2 layer is very close to the bulk hole concentration.

Under the trigonal ligand field, the Co 3d t_{2g} orbitals are split into the e'_g and a_{1g} orbitals, and the a_{1g} orbital is located at E_F and accommodates the holes in Li_xCoO_2. The Co 3d e'_g orbitals and the O 2p orbitals are fully occupied by electrons and form the valence band. The Fermi velocity of the Co 3d a_{1g} Fermi surface is estimated to be $\sim$ 0.46 eV$\mathring{A}$. Since the bare Fermi velocity of the a_{1g} is calculated to be $\sim$ 2 eV$\mathring{A}$ for x=0.46, [31, 35, 36] the renormalization factor is $\sim$ 4. In addition to the Co 3d a_{1g} band near E_F, another dispersive band is observed in the energy range from -0.3 eV to -0.8 eV and can be assigned to the Co 3d e'_g orbital. The energy width of the observed e'_g band dispersion (from -0.8 eV to -0.3 eV for 0.2 Å^{-1} to 0.7 Å^{-1} along the Γ-M direction) approximately agrees with the calculated result for $Na_{0.5}CoO_2$ without band renormalization (-1.0 eV to -0.5 eV for 0.2 Å^{-1} to 0.7 Å^{-1}) [36] in contrast to the strong renormalization of the a_{1g} band.

If the topmost CoO_2 layer has the same hole concentration as the bulk, the stacking

of $[CoO_2]^{-0.46}$ layer and $[Li_{0.46}]^{+0.46}$ layer should have polar catastrophe. In order to avoid the catastrophe, the hole concentration of the topmost layer may increase to $[CoO_2]^{-0.23}$, inconsistent with the present ARPES result. However, when single crystals are cleaved at the Li layer, it is natural to assume that half of the Li^+ ions remain on the measured surface while the other half of the Li^+ ions are on the other side of cleaved surface. If the Li^+ ions are homogeneously distributed on the surface, the top most layer is $[Li_{0.23}]^{+0.23}$ followed by the stacking of $[CoO_2]^{-0.46}$ layer and $[Li_{0.46}]^{+0.46}$ layer as illustrated in Fig. 1(c). In such case, the polar catastrophe can be avoided and the surface CoO_2 layer has the same hole concentration as the bulk.

If half of Li^+ ions remain at cleaved surface of LixCoO$_2$, polar catastrophe can be avoided without changing hole concentration of CoO_2 layers near the surface. For example, in $LiCoO_2$, the surface $[Li_{0.5}]^{+0.5}$ layer followed by stacking of $[CoO_2]^-$ and $[Li]^+$layers does not have polar catastrophe. In the STM study by Iwaya *et al.* for x=0.66, a small fraction of the cleaved surface was covered by Li with insulating subsurface CoO_2 layer while the other part was not covered by Li with metallic CoO_2 layer. [34] Assuming that the topmost Li and CoO_2 layers are modified from the bulk, their total charge should be -0.33. It is reasonable that the subsurface CoO_2 layer is insulating with $[CoO_2]^-$ when it is covered by $[Li_{0.66}]^{+0.66}$. Also the surface CoO_2 layer has higher hole concentration with $[CoO_2]^{-0.33}$ when it is not covered. If the surface of $Li_{0.46}CoO_2$ is covered by Li with inhomogeneous distribution just like x=0.66, half of the surface would be covered by $[Li_{0.5}]^{+0.5}$ and the underlying CoO_2 layer would be undoped and insulating. On the other hand, the other half of the surface is not covered by Li, and the topmost CoO_2 layer should be metallic with hole concentration higher than the bulk one. The excellent agreement of the observed Fermi surface area with the bulk hole concentration for x=0.46 indicates that the surface CoO_2 layer is dominated by the metallic region with the bulk hole concentration at x=0.46. Therefore, the situation at x=0.46 is inconsistent with the STM study for x=0.66.

Figure 3 exhibits a Fermi surface map for x=0.71 taken at $h\nu$ = 70 eV. The extrapolated Fermi surface is almost circular and can be fitted to a circle with radius of 0.67 $\pm$ 0.03 $\mathring{A}^{-1}$. Since the observed Fermi surface is hexagonally and elliptically distorted from an ideal circle, the upper limit of the radius is set to cover the Fermi surface while the circle with the radius in the lower limit is included in the Fermi surface. The small elliptic distortion is probably due to the transition matrix element effect since the spectral weight is strongly

suppressed around cut 5. The Fermi surface area is estimated to be $\sim 1.41 \pm 0.15$ $\AA^{-2}$ whereas that expected from the Li content is 0.83 $\AA^{-2}$. Again assuming that the Fermi surface does not depend on the out-of-plane wave number k_z, the area of the Fermi surface is much larger than that expected for the bulk. If the crystal is cleaved at the Li layer and half of the Li ions remain at the measured surface, the topmost layer is $[Li_{0.355}]^{+0.355}$ and is followed by the $[CoO_2]^{-0.71}$ layer and $[Li_{0.71}]^{+0.71}$ layer. In such case, the Fermi surface of the subsurface CoO_2 layer should be similar to that of the bulk. However, at x=0.71, the Fermi surface area larger than the expectation is probably consistent with the STM study for x=0.66. [34] Here, one can assume that the Li^+ ions are distributed inhomogeneously and that smaller fraction of the surface is covered by $[Li_{0.645}]^{+0.645}$ and the other part is covered by $[Li_{0.195}]^{+0.195}$. (The average should be close to $[Li_{0.355}]^{+0.355}$.) In order to keep the total charge of +0.355 at the topmost two layers for avoiding the polar catastrophe, the subsurface CoO_2 layer is undoped and insulating under the $[Li_{0.645}]^{+0.645}$ region while that under $[Li_{0.195}]^{+0.195}$ is $[CoO_2]^{-0.55}$ as shown in Fig. 1(d). The Fermi surface area of the $[CoO_2]^{-0.55}$ layer is expected to be about 1.3 $\AA^{-2}$ partly consistent with the experimental result.

Since the large Fermi surface area at x=0.71 is as large as that of x=0.46, the ARPES result would be consistent with electronic phase separation between x=0.0 and x=0.5. In order to examine this possibility, x dependence of the angle-integrated valence band spectra of x=0.71, 0.46, and 0.25 is shown in Fig. 4. The x=0.25 sample is metallic and exhibits substantial spectral weight at E_F as shown in Fig. 4. However, in ARPES measurements for x=0.25, the spectral weight at E_F does not show any momentum dependence, and no clear Fermi surface is observed. Here, the angle-integrated spectrum of x=0.25 is compared with those of x=0.71 and 0.46 which are integrated along the Γ-M direction. The Co 3d peak is systematically shifted towards the Fermi level with decreasing x or the hole doing in the CoO_2 layers indicating that the chemical potential is shifted downwards with the hole concentration. If the bulk of Li_xCoO_2 has electronic phase separation into hole-rich and hole-poor regions, the chemical potential is kept constant and the the volume fraction of of the hole-rich regions increases with the hole doping. Therefore, the monotonic chemical potential shift with x excludes possibility of the phase separation scenario. Here, we speculate that the inhomogeneous Li distribution at the surface is responsible for the deviation of the Fermi surface area at x=0.71. It is also interesting that the Co 3d peak width of x=0.46 is

smaller than that of x=0.71. This observation is probably consistent with the homogeneous (inhomogeneous) distribution of Li in x=0.46 (x=0.71).

The Fermi velocity is $\sim$ 0.56 eV$\mathring{A}$ for x=0.71 which is slightly enhanced from that for x=0.46, indicating that the renormalization factor is $\sim$ 3. The e'_g band is observed in the energy range from -0.4 eV to -0.9 eV. The energy width of the observed e'_g band dispersion (from -0.9 eV to -0.4 eV for 0.2 $\mathring{A}^{-1}$ to 0.7 $\mathring{A}^{-1}$ along the Γ-M direction) approximately agrees with the calculated result for $Na_{0.5}CoO_2$ without band renormalization (-1.0 eV to -0.5 eV for 0.2 $\mathring{A}^{-1}$ to 0.7 $\mathring{A}^{-1}$) [36] indicating that the renormalization factor is almost 1. As predicted by the calculation [36], the band dispersion of the e'_g band becomes very steep near the Γ point and is not clearly observed in the experimental results.

As shown in Fig. 4, the valence-band peak is shifted towards E_F consistent with the hole doping. Considering the Fermi velocity estimated from the ARPES result, the energy shift is estimated to be $\sim$ 0.1 eV per 0.1 hole. Such a large chemical potential shift is inconsistent with the small Fermi velocity observed for the a_{1g} band, indicating anomalous metallic state of Li_xCoO_2. Without the renormalization effect, the a_{1g} band is almost flat for $k_x < 0.5$ $\mathring{A}^{-1}$ and becomes steep for $k_x > 0.5$ $\mathring{A}^{-1}$. Therefore, for $x < 0.6$ with $k_F > 0.5$ $\mathring{A}^{-1}$, the large chemical potential shift is consistent with the bare band dispersion before the renormalization [31] while the a_{1g} band is strongly renormalized with renormalization factor of 3-4. The shoulder structure at $\sim$ -0.3 eV can be assigned to the bottom of a_{1g} band and the top of e'_g band. The main peak at $\sim$ 1eV can be assigned to the incoherent weights of the a_{1g} and e'_g bands due to strong electron-electron or electron-lattice interactions. In particular, since O 2p components are heavily mixed into the Co 3d states near E_F, the electron-lattice interaction can be enhanced by strong coupling with Co-O lattice distortions.

Figures 5(a) and 5(b) show band maps of the entire valence band taken at $h\nu$ = 70 eV approximately along Γ-M for x=0.46 and x=0.71, respectively. The band maps are compared with the calculated band dispersions for $LiCoO_2$ by Czyżyk, Potze, and Sawatzky. [25] The structure at $\sim$ -1 eV with small band dispersion can be assigned to the incoherent part of the Co 3d a_{1g} and e'_g bands while the broad band ranging from -2 eV to -6 eV to the O 2p band. Compared to the dispersive Co 3d a_{1g} and e'_g bands in Figs. 2 and 3, the incoherent Co 3d band is very broad with small dispersion. The dispersive Co 3d e'_g band is located at $\sim$ -0.9 eV around the zone center and is moved to $\sim$ -0.4 eV at its band maximum for x=0.71 (Fig. 3). As for x=0.46, it is located at $\sim$ -0.8 eV around the zone center and is moved to $\sim$ -0.3

eV at its band maximum (Fig. 2). The energy shift between x=0.71 and x=0.46 is consistent with the chemical potential shift suggested from Fig. 4. Interestingly, the incoherent Co 3d band exhibits small dispersion of $\sim$ 0.1 eV in going from the zone center to the zone boundary. The dispersion of the incoherent component would be related to incoherent hopping transport of Co^{4+} species in background of low-spin Co^{3+} as suggested in other triangular-lattice Co oxides. [11] This picture is consistent with the observation of Co^{4+} and Co^{3+} peaks in the O 1s XAS spectra [32] as well as the strong charge fluctuation suggested by recent theoretical [37] and optical [38] studies. The present ARPRES study shows that the x=0.46 sample exhibits homogeneous electronic states compared to the in homogeneous x=0.71. Here, a challenging question is how one can understand the coexistence of the incoherent Co^{4+}/Co^{3+} components and the coherent Femi surface beyond a simple phase separation picture.

IV. CONCLUSION

We have studied the electronic structure of Li_xCoO_2 single crystals by means of ARPES. The Co 3d a_{1g} band crosses E_F with strongly renormalized band dispersion while the Co 3d e'_g bands are fully occupied without renormalization in Li_xCoO_2. The area of the a_{1g} Fermi surface is consistent with the hole concentration at x=0.46 indicating that the ARPES results represent the bulk electronic structure and that the surface charge redistribution is unlikely. At x=0.71, the Fermi surface area is larger than the expectation which can be associated to the inhomogeneous distribution of Li and the surface charge redistribution for avoiding polar catastrophe. Since the Co 3d peak is systematically shifted with x, the possibility of phase separation between hole-rich and hole-poor regions is excluded. Therefore, the coexistence of the a_{1g} Fermi surface and the incoherent Co 3d peak $\sim$ 1 eV below E_F indicates strong electron-electron and electron-lattice interactions in the present system.

Acknowledgement

This work was partially supported by Grants-in-Aid from the Japan Society of the Promotion of Science (JSPS) and CREST (JPMJCR15Q2) from the Japan Science and Technology Agency (JST). The synchrotron radiation experiment was performed with the approval of

Photon Factory, KEK (2015G058).

[1] K. Mizushima, P. C. Jones, P. J. Wiseman, and J. B. Goodenough, Mater. Res. Bull. **15**, 783 (1980).

[2] E. Plichta, S. Slane, M. Uchiyama, M. Salomon, D. Chua, W. B. Ebner, and H. W. Lin, J.Electrochem. Soc. **136**, 1865 (1989).

[3] H. F. Gibbard. J.Power Sources **26**, 81 (1989).

[4] T. Nagura and K. Tazawa, Prog. Batteries Sol. Cells **9**, 20 (1990).

[5] X. Wang, I. Loa, K. Kunc, K. Syassen, and M. Amboage, Phys. Rev. B **72**, 224102 (2005).

[6] I. Terasaki, Y. Sasago, and K. Uchinokura, Phys. Rev. B **56**, R12685 (1997).

[7] K. Takada, H. Sakurai, E. Takayama-Muromachi, F. Izumi, R. A. Dilanian, and T. Sasaki, Nature (London) **422**, 53 (2003).

[8] M. L. Foo, Y. Wang, S. Watauchi, H. W. Zandbergen, T. He, R. J. Cava, and N. P. Ong, Phys. Rev. Lett. **92**, 247001 (2004).

[9] K. Miyoshi, E. Morikuni, K. Fujiwara, J. Takeuchi, and T. Hamasaki, Phys. Rev. B **69**, 132412 (2004).

[10] T. Motohashi, R. Ueda, E. Naujalis, T. Tojo, I. Terasaki, T. Atake, M. Karppinen, and H. Yamauchi, Phys. Rev. B **67**, 064406 (2003).

[11] T. Mizokawa, L. H. Tjeng, P. G. Steeneken, N. B. Brookes, I. Tsukada,T. Yamamoto, and K. Uchinokura, Phys. Rev. B **64**, 115104 (2001).

[12] T. Mizokawa, L. H. Tjeng, H.-J. Lin, C. T. Chen, R. Kitawaki, I. Terasaki, S. Lambert, and C. Michel, Phys. Rev. B **71**, 193107 (2005).

[13] W. B. Wu, D. J. Huang, J. Okamoto, A. Tanaka, H. J. Lin, F. C. Chou, A. Fujimori, and C. T. Chen, Phys. Rev. Lett. **94**, 146402 (2005).

[14] M. Z. Hasan, Y. D. Chuang, D. Qian, Y. W. Li, Y. Kong, A. P. Kuprin, A. V. Fedorov, R. Kimmerling, E. Rotenberg, K. Rossnagel, Z. Hussain, H. Koh, N. S. Rogado, M. L. Foo, and R. J. Cava, Phys. Rev. Lett. **92**, 246402 (2004).

[15] H. B. Yang, S. C. Wang, A. K. P. Sekharan, H. Matsui, S. Souma, T. Sato, T. Takahashi, T. Takeuchi, J. C. Campuzano, R. Jin, B. C. Sales, D. Mandrus, Z. Wang, and H. Ding, Phys. Rev. Lett. **92**, 246403 (2004).

[16] H. B. Yang, Z. H. Pan, A. K. P. Sekharan, T. Sato, S. Souma, T. Takahashi, R. Jin, B. C. Sales, D. Mandrus, A. V. Fedorov, Z. Wang, and H. Ding, Phys. Rev. Lett. **95**, 146401 (2005).

[17] D. Qian, L. Wray, D. Hsieh, L. Viciu, R. J. Cava, J. L. Luo, D. Wu, N. L. Wang, and M. Z. Hasan, Phys. Rev. Lett. **97**, 186405 (2006).

[18] J. Geck, S. V. Borisenko, H. Berger, H. Eschrig, J. Fink, M. Knupfer, K. Koepernik, A. Koitzsch, A. A. Kordyuk, V. B. Zabolotnyy, and B. Büchner, Phys. Rev. Lett. **99**, 046403 (2007).

[19] T. Shimojima, K. Ishizaka, S. Tsuda, T. Kiss, T. Yokoya, A. Chainani, S. Shin, P. Badica, K. Yamada, and K. Togano, Phys. Rev. Lett. 97, 267003 (2006).

[20] T. Arakane, T. Sato, T. Takahashi, H. Ding, T. Fujii, and A. Asamitsu, J. Phys. Soc. Jpn. **76**, 054704 (2007).

[21] T. Arakane, T. Sato, T. Takahashi, T. Fujii, and A. Asamitsu, Phys. Rev. B **81**, 115132 (2010).

[22] T. Arakane, T. Sato, T. Takahashi, T. Fujii, and A. Asamitsu, New J. Phys. **13**, 043021 (2011).

[23] T. A. Hewston and B. Chamberland, J. Phys. Chem. Solids **48**, 97 (1987), and references cited therein.

[24] J. van Elp, J. L. Wieland, H. Eskes, P. Kuiper, G. A. Sawatzky, F. M. F. de Groot, and T. S. Turner, Phys. Rev. B **44**, 6090 (1991).

[25] M. T. Czyżyk, R. Potze, and G. A. Sawatzky, Phys. Rev. B **46**, 3729 (1992).

[26] I. Tomeno and M. Oguchi, J. Phys. Soc. Jpn **67**, 318 (1998).

[27] M. Ménétrier, I. Saadoune, S. Levasseur, and C. Delmas, J. Mater. Chem. **9**, 1135 (1999).

[28] J. T. Hertz, Q. Huang, T. McQueen, T. Klimczuk, J. W. G. Bos, L. Viciu, and R. J. Cava, Phys. Rev. B **77**, 075119 (2008).

[29] K. Miyoshi, H. Kondo, M. Miura, C. Iwai, K. Fujiwara, and J. Takeuchi, J. Phys. Conference Series **150**, 042129 (2009).

[30] K. Miyoshi, C. Iwai, H. Kondo, M. Miura, S. Nishigori, and J. Takeuchi, Phys. Rev. B **82**, 075113 (2010).

[31] K. Ikedo, Y. Wakisaka, T. Mizokawa, C. Iwai, K. Miyoshi, and J. Takeuchi, Phys. Rev. B **82**, 075126 (2010).

[32] T. Mizokawa, Y. Wakisaka, T. Sudayama, C. Iwai, K. Miyoshi, J. Takeuchi, H. Wadati, D. G.

Hawthorn, T. Z. Regier, and G. A. Sawatzky Phys. Rev. Lett. **111**, 056404 (2013).

[33] L. Simonelli, E. Paris, C. Iwai, K. Miyoshi, J. Takeuchi, T. Mizokawa, N. L. Saini, J. Phys. Condens. Matter **29**, 105702 (2017). .

[34] K. Iwaya, T. Ogawa, T. Minato, K. Miyoshi, J. Takeuchi, A. Kuwabara, H. Moriwake, Y. Kim, and T. Hitosugi Phys. Rev. Lett. **111**, 126104 (2013).

[35] K. Ikedo, Y. Wakisaka, T. Mizokawa, C. Iwai, K. Miyoshi, and J. Takeuchi, J. Phys. Soc. Jpn. **78**, 063707 (2009).

[36] D. J. Singh, Phys. Rev. B **61**, 13397 (2000).

[37] E. B. Isaacs and C. A. Marianetti, Phys. Rev. B **95**, 045141 (2017).

[38] H. L. Liu, T. Y. Ou-Yang, H. H. Tsai, P. A. Lin, H. T. Jeng, G. J. Shu, and F. C. Chou, New J. Phys. **17**, 103004 (2015).

Figure captions

Figure 1: (Color online) (a) Schematic drawing of CoO_2 layer. The CoO_6 octahedra share their edges. (b) Electronic configurations for Co_{3+} (d^6) and Co_{4+} (d^5) . (c) Stacking of Li and CoO_2 layers for x=0.46 with homogeneous Li distribution at surface. The dashed line indicates the surface layer where half of Li^+ ions remain. (d) Stacking of Li and CoO_2 layers for x=0.71 with inhomogeneous Li distribution at surface. The surface layer consists of the $[Li_{0.645}]^{+0.645}$ region and the $[Li_{0.195}]^{+0.195}$ region (indicated by the dashed line). In order to keep the total charge of +0.355 in the topmost two layers, the subsurface CoO_2 layer is undoped and insulating (indicated by the thick line) under the $[Li_{0.645}]^{+0.645}$ region and is metallic with larger hole concentration under the $[Li_{0.195}]^{+0.195}$ region.

Figure 2: (Color online) (a)Fermi surface map at $h\nu$ = 70 eV for x=0.46 (20 K) and (b) band maps along the cuts indicated in the Fermi surface map. The Fermi surface map is obtained by plotting ARPES intensity integrated within ±5 meV from the Fermi level as a function of in-plane wave numbers k_x and k_y. The band maps are obtained by plotting second derivatives of momentum distribution curves as a function of energy and wave number along the cuts. (c) Band map near the Fermi surface. The squares indicate the band positions obtained by fitting momentum distribution curves to Gaussians. The line indicates the least squares fit for the band positions.

Figure 3: (Color online) (a) Fermi surface map at $h\nu$ = 70 eV for x=0.71 (20 K) and (b) band maps along the cuts indicated in the Fermi surface map. The solid lines in the Fermi surface map show the Brillouin zone boundaries. The Fermi surface map is obtained by plotting ARPES intensity integrated within ±5 meV from the Fermi level as a function of in-plane wave numbers k_x and k_y. The band maps are obtained by plotting second derivatives of momentum distribution curves as a function of energy and wave number along the cuts. (c) Band map near the Fermi surface. The squares indicate the band positions obtained by fitting momentum distribution curves to Gaussians. The line indicates the least squares fit for the band positions.

Figure 4: (Color online) Angle-integrated photoemission spectra of x=0.71, 0.46, and 0.25.

Figure 5: (Color online) Band maps of the entire valence band at $h\nu$ = 70 eV approximately along Γ-M for (a) x=0.46 and (b) x=0.71. The dot-dash curves indicate the calculated band dispersions for $LiCoO_2$ by Czyżyk, Potze, and Sawatzky. [25]

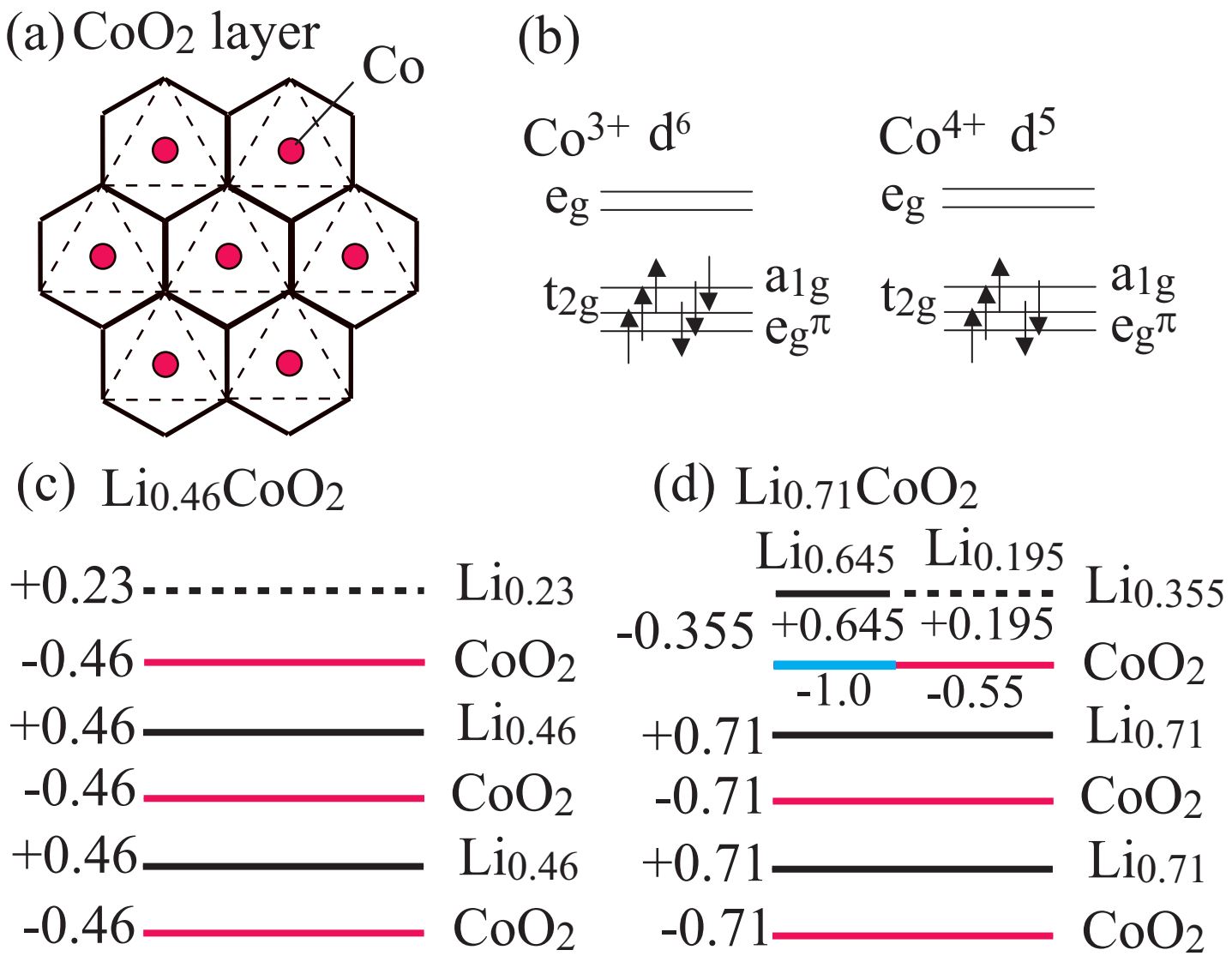

Figure 1 02Aug2017

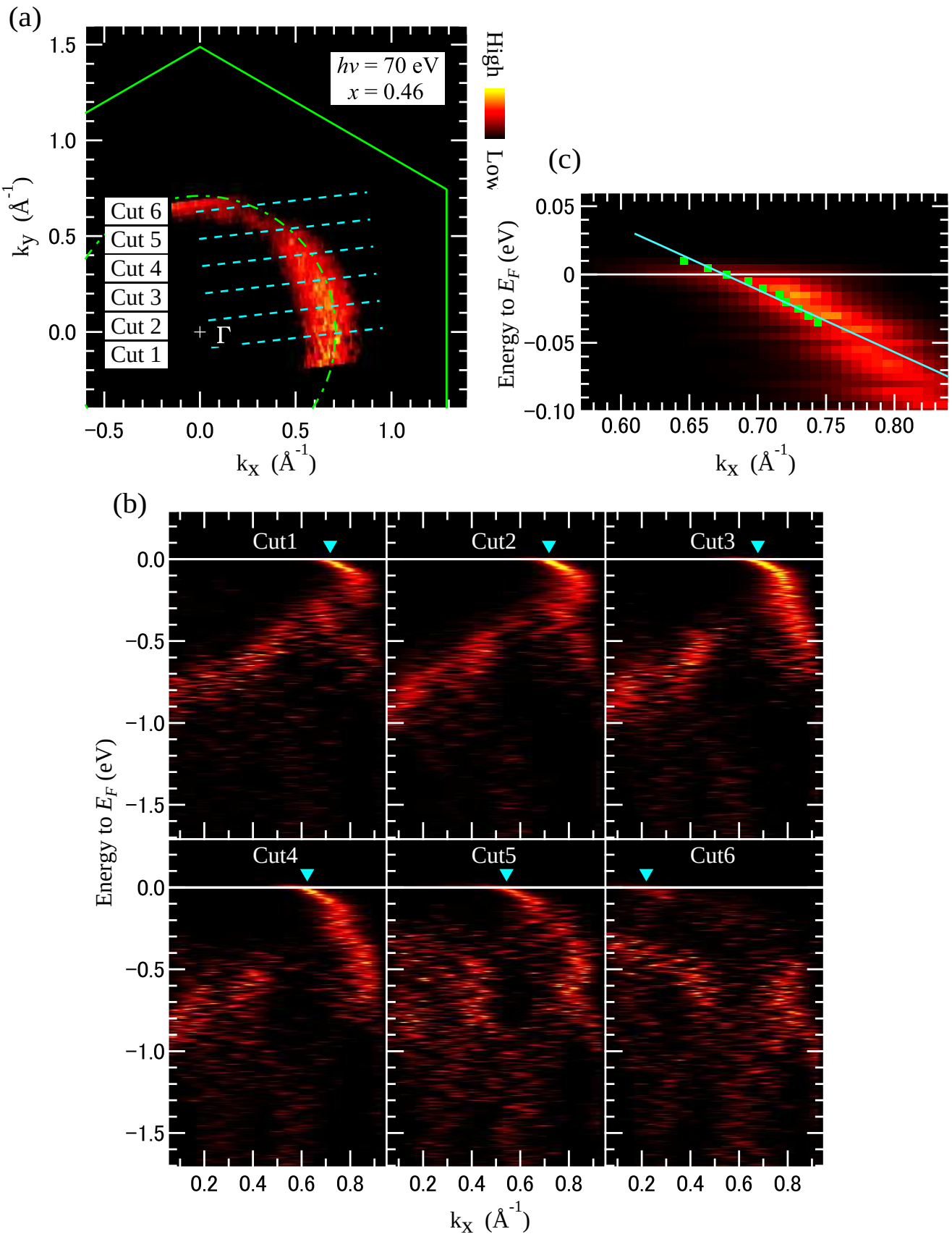

Figure 2 02Aug2017

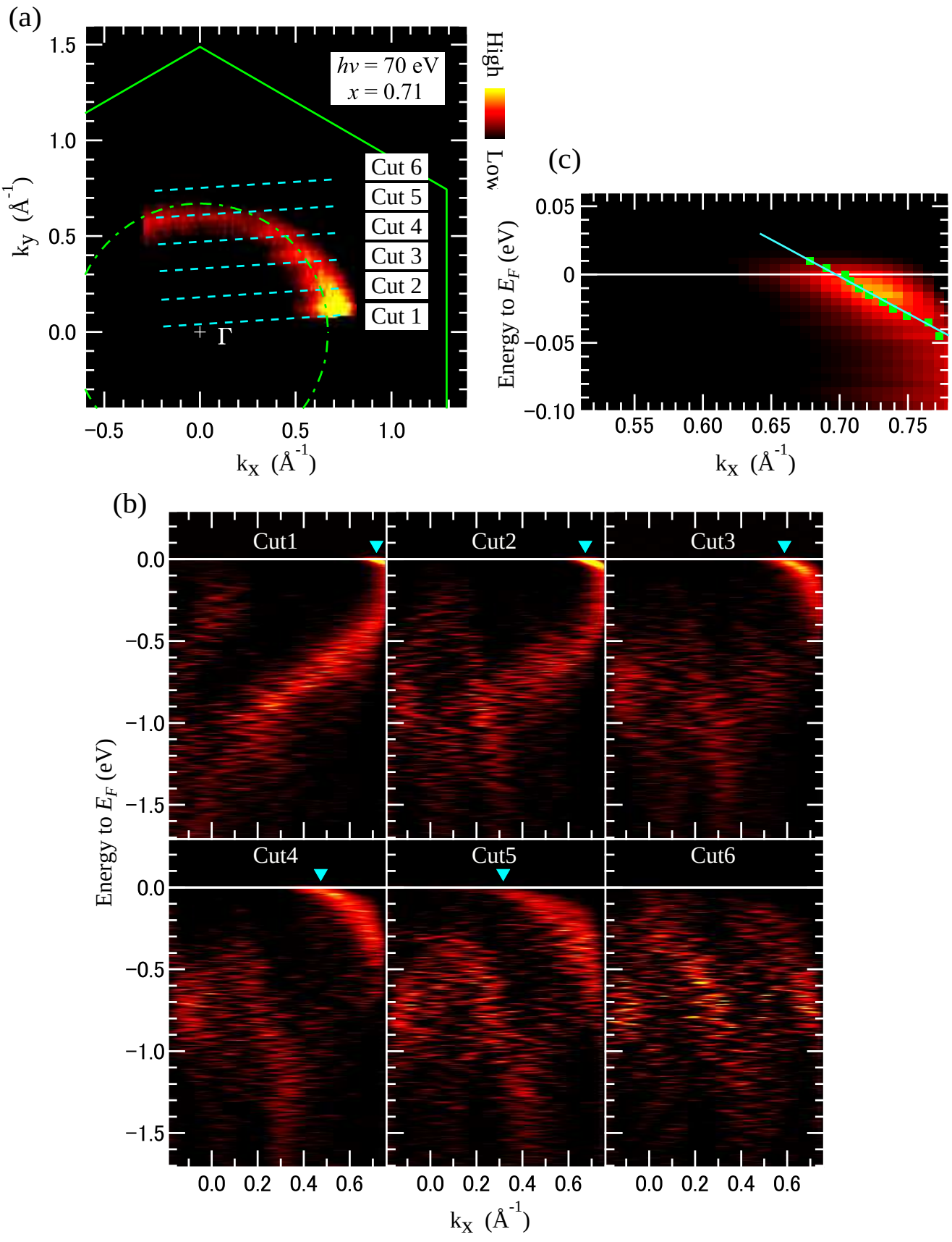

Figure 3 02Aug2017

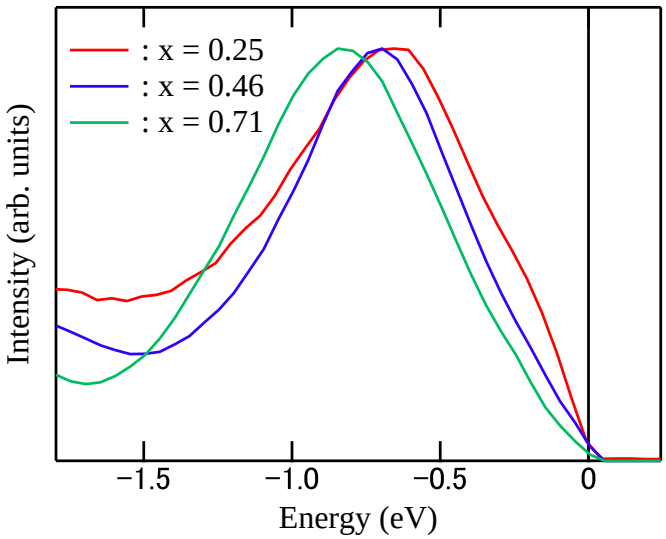

Figure 4 02Aug2017

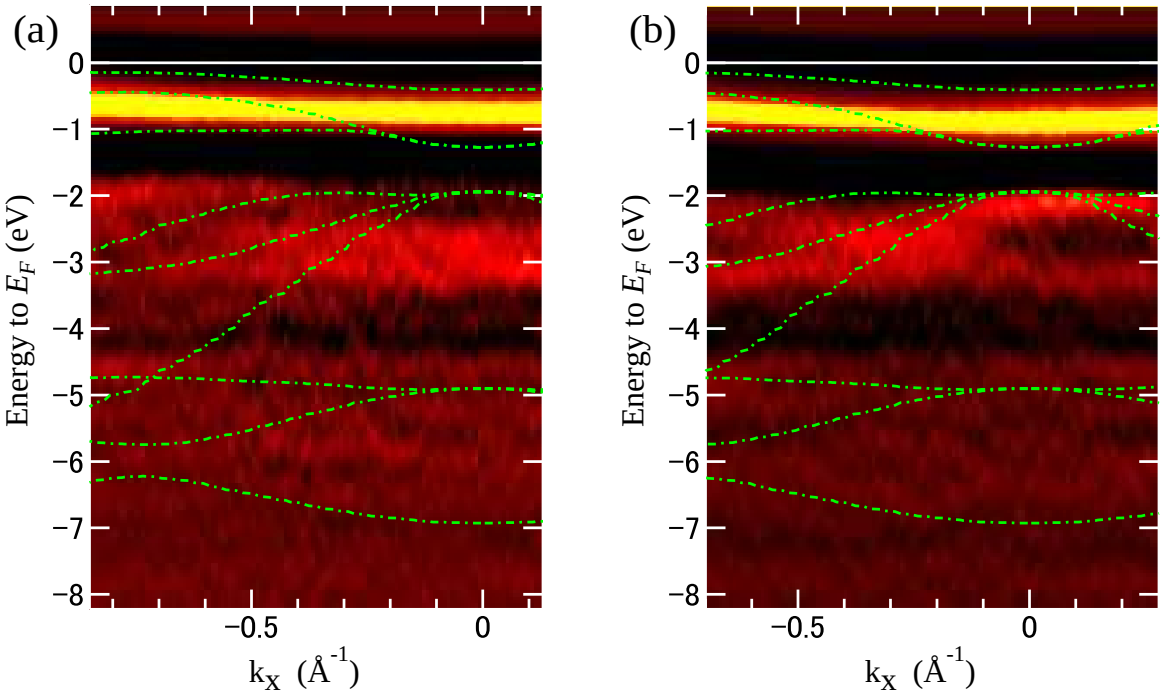

Figure 5 02Aug2017